Title
Analysis of illumination coherence properties in small-source systems such as synchrotrons

Journal
Applied Optics, 42(14)

Authors
Chang, Chang
Naulleau, Patrick
Attwood, David

Publication Date
2002-09-20

Analysis of illumination coherence properties in small-source systems such as synchrotrons

Chang Chang[1,2], Patrick Naulleau[1], David Attwood[1,2]

[1]Center for X-Ray Optics,

Lawrence Berkeley National Laboratory, Berkeley, CA 94720

[2]Department of Electrical Engineering & Computer Sciences,

University of California, Berkeley, CA 94720

cnchang@lbl.gov

Modern synchrotron beamlines often take the form of critical illumination systems, where an incoherent source of limited spatial extent is re-imaged to an experimental plane of interest. Unique constraints of synchrotron sources and beamlines, however, may preclude the use of the simple Zernike approximation for calculating the object-image coherence relationship. Here, we perform a rigorous analysis of the object-image coherence relationship valid for synchrotron beamlines. The analysis shows beamline aberrations to have an effect on the coherence properties. Effects of various low-order aberrations on the coherence properties are explicitly studied.

OCIS codes: 999.9999, 000.0000 Fill in OCIS codes here.

1. Introduction

Through spatial and spectral filtering, high brightness and high coherent power undulators available at third generation synchrotron radiation facilities enable a variety of experiments that require a high degree of coherence at short wavelengths. Undulator sources are regarded as incoherent because the electrons in the synchrotron storage ring have uncorrelated motion and thus are essentially independent radiators. Beamline optics are routinely used to re-image this spatially confined incoherent source to an experimental plane of interest. Such a configuration is readily recognized as a critical illumination system [1], where the beamline acts as the condenser.

Undulator radiation has an intrinsic divergence angle, known as the central radiation cone angle θ_{cen}, characterized by the electron forward-emitting radiation [2]. The beamline acceptance angle, i.e. object-side numerical aperture (NA) of the condenser, is usually set to be comparable but slightly smaller than θ_{cen}. This acceptance angle sets the effective coherence patch size on the source as seen by the condenser system. For the Van Cittert-Zernike theorem to correctly predict the spatial coherence distribution at the image plane of the condenser, the dimension of the source must be much greater than this effective coherence patch size, i.e.

$$d_{source} \gg d_{coh}^{eff} \approx \frac{1}{2\pi} \frac{\lambda}{\theta_{accept}} \tag{1}$$

where d_{source} is the source dimension, d_{coh}^{eff} is the effective coherence patch size at the source, λ is the wavelength, and θ_{accept} is the beamline acceptance angle. However, the distinct characteristics of third generation undulator radiation, i.e. the small vertical source dimension

and the constraint on the size of beamline acceptance angle, give rise to a condenser system whose spatial coherence properties cannot be simplified by the commonly used Zernike approximation [1, 3, 4]. For the $\lambda = 13.4\,nm$ application considered here, the Gaussian undulator source has a vertical dimension (2σ) of $d_{source} = 32\,\mu m$, and the beamline acceptance angle is $\theta_{accept} = 48\,\mu rad$, smaller than the central radiation cone angle of $80\,\mu rad$. The d_{coh}^{eff} thus equals to $45\,\mu m$, for which Eq.(1) is clearly not satisfied and the Zernike approximation is not applicable.

Here, based on the Huygens-Fresnel principle, the analysis and numerical evaluation of the spatial coherence properties of a representative undulator beamline are presented and the results are compared with measurements conducted at Lawrence Berkeley National Laboratory's Advanced Light Source undulator beamline 12. Moreover, the effects of beamline aberrations on coherence properties are studied.

2. Rigorous mutual coherence propagation for undulator beamlines

A. Undulator radiation as an incoherent source

Synchrotron-based undulator sources can be approximated as incoherent under the condition that the coherence width at the source is smaller than the diffraction-limited resolution of the condenser (i.e. beamline). Alternatively, this could be stated as requiring the intrinsic divergence of the source to be larger than the acceptance angle of the beamline. For the undulator source, the positions and motion of the electrons in the undulator are uncorrelated. All point radiators originating from uncorrelated electrons can be treated as independent, and the effective size of an elemental point radiator can be determined from the central radiation cone divergence [2]. The intrinsic divergence of the extreme ultraviolet (EUV)

undulator considered here [7] is $\theta_{cen} = 80\,\mu rad$, which is larger than the beamline acceptance angle θ_{accept} of $48\,\mu rad$. Therefore, it is evident that the incoherent source approximation holds.

B. Zernike approximation for a condenser system

The Zernike approximation, first described by F. Zernike in 1938 [4], states that the condenser lens pupil, when illuminated by a large incoherent source, can be regarded as a secondary incoherent source whose intensity distribution is given by the modulus square of the pupil function. This approximation, described again by Born & Wolf [3] (sec.10.5.2) and Goodman [1] (sec.7.2.2), is commonly used for condensers operating at visible wavelengths.

Starting with an incoherent source placed at the object plane of the condenser, the Van Cittert-Zernike theorem [3, 1, 4] can be used to propagate this incoherent source to the condenser lens pupil and the resultant mutual intensity at the condenser lens is given by a Fourier transform of the source intensity distribution. The condition under which the Zernike approximation is valid requires that the incoherent source subtends a sufficiently large angle at the condenser lens, such that the coherence width at the condenser lens is small relative to the pupil diameter. Satisfying this condition, the condenser lens pupil can be regarded as a secondary source with a small coherence area and the generalized Van Cittert-Zernike theorem [1] can then be used to propagate the mutual intensity from the condenser lens pupil to the image plane of the condenser. The resultant coherence distribution at the image plane of the condenser is thus determined solely by the modulus square of the pupil function and aberrations in the condenser lens do not affect the coherence distribution at the image plane.

However, when the dimension of the incoherent source shrinks to the point where the coherence width at the condenser lens is comparable to the pupil diameter, the Zernike approximation fails and the generalized Van Cittert-Zernike theorem can no longer be used to propagate the mutual intensity function from the exit of the condenser lens to the image-plane. Under this small-source condition, a rigorous mutual coherence propagation based on the Huygens-Fresnel principle is required [1]. As will be shown here, in this case, the condenser pupil aberrations begin to affect the coherence properties at the condenser image-plane.

C. Undulator beamline as a condenser: an example

Undulator Beamline 12, operational at Lawrence Berkeley National Laboratory's Advanced Light Source synchrotron radiation facility can be viewed as an incoherent source with a Gaussian intensity distribution, $(\sigma_\xi, \sigma_\eta) = (260\mu m, 16\mu m)$. The beamline essentially acts as a condenser lens with a de-magnification of 60 and an object-side NA of $48\,\mu rad$. The distance z_1 from the undulator source plane to the pupil is $16.7\,m$ and the pupil radius a is $0.8\,mm$. The wavelength used here is $\lambda = 13.4\,nm$.

Using the Van Cittert-Zernike theorem to propagate radiation from the incoherent source to the lens pupil, the mutual intensity at the pupil is given by a Fourier transform of the Gaussian intensity distribution of the incoherent undulator source. The resultant coherence distribution at the pupil is then Gaussian distributed with rms radii

$$(\sigma_x^C, \sigma_y^C) = (\frac{\lambda z_1}{2\pi\sigma_\xi}, \frac{\lambda z_1}{2\pi\sigma_\eta}) \approx (0.14\,mm, 2.23\,mm). \tag{2}$$

Comparing the vertical size of this coherence patch with the pupil diameter ($2a = 1.6\,mm$), the Zernike approximation is found not to be applicable and, therefore, the generalized

Van Cittert-Zernike theorem cannot be used to propagate the mutual coherence from the condenser pupil to the image-plane. However, should this invalidity be ignored, and the Zernike approximation be used for the calculation of the spatial coherence distribution at the condenser image-plane, the erroneous resultant coherence distribution would be calculated to be an Airy pattern with a first null radius s_o of $2.84\,\mu m$. Noting that this radius is approximately equal to the expected coherence patch size. This over-simplification results in discrepancy with the experimentally measured coherence profile [5], which determined the size of the coherence patch to be $4.4\,\mu m$ and $6.8\,\mu m$ in the horizontal and vertical direction, respectively.

As demonstrated, the generalized Van Cittert-Zernike theorem does not apply for the undulator case of interest here, and a more rigorous coherence analysis is required.

3. Object-image coherence relation

Using the Huygens-Fresnel principle [1], the object-image coherence relation, under quasi-monochromatic and paraxial approximations, can be expressed as

$$\mathbf{J}_i(u_1,v_1;u_2,v_2) = \iiiint_{-\infty}^{+\infty} \mathbf{J}_o(\xi_1,\eta_1;\xi_2,\eta_2)\mathbf{K}(u_1,v_1;\xi_1,\eta_1)\mathbf{K}^*(u_2,v_2;\xi_2,\eta_2)d\xi_1 d\eta_1 d\xi_2 d\eta_2 \quad (3)$$

where $\mathbf{J}_i$ and $\mathbf{J}_o$ are the mutual intensities at the image and object plane, respectively. The *amplitude spread function* $\mathbf{K}$ is defined by

$$\begin{aligned}\mathbf{K}(u,v;\xi,\eta) = {} & \frac{\exp\left\{j\frac{\pi}{\lambda z_2}(u^2+v^2)\right\}\exp\left\{j\frac{\pi}{\lambda z_1}(\xi^2+\eta^2)\right\}}{\lambda^2 z_2 z_1} \\ & \times \iint_{-\infty}^{+\infty} \mathbf{P}(x,y)\exp\left\{-j\frac{2\pi}{\lambda z_2}\left[\left(u+\frac{z_2}{z_1}\xi\right)x+\left(v+\frac{z_2}{z_1}\eta\right)y\right]\right\}dxdy\end{aligned} \quad (4)$$

where $\mathbf{P}(x,y)$ is the complex pupil function. The coordinate system used throughout this paper is depicted in Fig. 1. Notice that the subscript i for (u_i,v_i) and (ξ_i,η_i) is dropped in

Eq.(4) for ease of notation.

If an incoherent source is placed at the object plane, then $\mathbf{J}_o$ can be written as

$$\mathbf{J}_o = \kappa\, I_s(\xi,\eta)\ \delta(\Delta\xi, \Delta\eta) \tag{5}$$

where $I_s(\xi,\eta)$ is the source intensity distribution, $\kappa = \lambda^2/\pi$, and $\delta(\cdot,\cdot)$ is a 2-dimensional Dirac delta function.

In this case, Eq.(3) simplifies to

$$\mathbf{J}_i(u_1,v_1;u_2,v_2) = \kappa \iint_{-\infty}^{+\infty} I_s(\xi,\eta)\mathbf{K}(u_1,v_1;\xi,\eta)\mathbf{K}^*(u_2,v_2;\xi,\eta)d\xi d\eta \tag{6}$$

The mutual intensity function $\mathbf{J}_i$ at the image plane can now be determined by the integration of the source intensity distribution I_s and the two off-centered [by (u_1,v_1) and (u_2,v_2), respectively] amplitude-spread functions of the pupil $\mathbf{P}$.

In order to simplify the notation in Eq.(6), we define

$$\mathbf{G}(u',v') \equiv \iint_{-\infty}^{+\infty} \mathbf{P}(x,y)\exp\left\{-j\frac{2\pi}{\lambda z_2}\Big[u'x+v'y\Big]\right\}dxdy \tag{7}$$

Note that $\mathbf{G}(u',v')$ is essentially the Fourier transform (up to a scaling constant) of the pupil $\mathbf{P}(x,y)$, i.e. the condenser point-spread function (PSF). Eq.(6) can now be written as

$$\begin{aligned}\mathbf{J}_i(u_1,v_1;u_2,v_2) = {} & \frac{\kappa\exp\left\{j\frac{\pi}{\lambda z_2}\,(u_1^2+v_1^2-u_2^2-v_2^2)\right\}}{\lambda^4 z_2^2 z_1^2} \\ & \times \iint_{-\infty}^{+\infty} I_s(\xi,\eta)\ \mathbf{G}\big(u_1+M\xi, v_1+M\eta\big)\mathbf{G}^*\big(u_2+M\xi, v_2+M\eta\big)d\xi d\eta,\end{aligned} \tag{8}$$

The mutual intensity can be obtained by numerically evaluating the above double integral. Equation (8), and its equivalent Eq.(6), are based on the Huygens-Fresnel principle and are valid regardless of the Zernike approximation. Note here that the mutual intensity is a function of the four individual coordinates, (u_1,v_1,u_2,v_2), not their differences.

The numerical value of $\mathbf{G}(u', v')$ can be determined by evaluating the integral in Eq.(7). This integral can be expressed as weighed summations of various Bessel functions for the specific aberrations involved [3, 6]. Here we explore the effects of defocus/distortion, astigmatism, and coma on the spatial coherence distributions at the condenser image plane.

4. Numerical evaluation results

Using the object-image coherence relation derived in Sec. 3, i.e. Eq.(8), the mutual intensity at the image plane of the condenser can now be determined numerically by incorporating the appropriate PSFs [i.e. $\mathbf{G}(u', v')$]. To test the validity of the numerical evaluation, a large ($1.6\,mm \times 1.6\,mm$) uniform intensity incoherent source is used to illuminate the condenser. Unlike the undulator source, this large square incoherent source can be shown to satisfy the Zernike approximation. The resultant intensity and coherence distributions with various pupil aberrations are shown in Fig. 2. As expected under the Zernike approximation, the various aberrations have negligible effect on the spatial coherence distributions, which are all essentially Airy patterns with first null radius of $2.8\,\mu m$. The intensity distributions are all relatively uniform, again as expected by the Zernike approximation. In the case of coma, the intensity distribution is shifted because the center of mass of the modulus square of the coma PSF is off-centered.

Next, an actual undulator source having a size that does not satisfy the Zernike approximation is studied. The intensity distribution of this incoherent undulator source is Gaussian with $(\sigma_x, \sigma_y) = (260\mu m, 16\mu m)$, given by the undulator beam size at the exit-plane. First, an aberration-free condenser is assumed in order to determine the effect of smaller source size. Figure 3 shows the failure of Zernike approximation for small sources, as the coherence

distribution deviates significantly from an Airy pattern.

It has been shown above that the size of the incoherent source has affected the coherence distribution at the image plane of a *critical* condenser and the apodized pupil function is not the sole determining factor. Next, the effect of pupil aberrations on the spatial coherence distribution is investigated. Several low order aberrations will be assumed in the condenser to demonstrate this effect. The PSFs required by Eq.(8) are given in Ref.[3] for defocus and distortion, and in Ref.[6] for astigmatism and coma. Figure 4 shows that in the case of smaller source size, the effect of condenser aberrations on spatial coherence cannot be ignored. With 0.5 waves of defocus in the condenser, the intensity and coherence distributions at the condenser-image plane is shown in Fig. 4(a). Figures 4(b) and (c) show the distributions under 0.5 waves of astigmatism and coma, respectively. For the cases of defocus and astigmatism, the high vertical coherence shown in Fig. 4(a) and (b) can be explained by the small vertical source size. However, in general the two dimensional coherence distributions cannot be treated separately in terms of vertical and horizontal directions. As demonstrated in the case of coma, shown in Fig. 4(c), the two dimensional structure of coma dominates the spatial coherence distribution in the condenser image-plane and the coherence distribution cannot be explained simply by the vertical and horizontal source size.

Noting that the coherence distribution is not simply a function of the difference of the coordinates, instead, it is a function of the four individual coordinates, i.e. (u_1, v_1, u_2, v_2). Therefore, when displaying the coherence distribution, one of the coordinates is fixed at the origin, i.e. $(u_1, v_1) = (0, 0)$, and the coherence distribution is obtained as the correlation factor $|\boldsymbol{\mu}_{12}|$ between various points (u_2, v_2) and the origin $(0, 0)$.

5. Discussion

As previously demonstrated experimentally [5], the Zernike approximation has been analytically shown to not hold for a typical EUV undulator beamline. Using the Zernike approximation significantly underestimates the coherence area, and hence the available coherent power. This can have important ramifications for experiments requiring coherence. For example, in speckle dynamics experiments [8] where coherent power is important but wavefront quality is typically not, it is evident that the Zernike approximation would significantly underestimate the usable beam size and power. We note, however, that for EUV point-diffraction interferometry [9, 10], these issues are less important. In this case, the spatial-filtering pinhole placed at the focus of the beamline serves the dual purpose of improving the spatial coherence, and, more importantly, generating a highly spherical probe beam. Even if the coherence area is larger than predicted, the pinhole size cannot be increased because doing so would adversely affect wavefront quality at the same time it increases the available coherent power.

We note that the results obtained here are valid for any condenser system that reimages an incoherent source to its conjugate plane (critical illumination), regardless of the Zernike approximation. We have demonstrated that for a condenser system employing an EUV undulator as the radiation source, the commonly used Zernike approximation is violated and numerical spatial coherence propagation based on Huygens-Fresnel principle is required. We note that the validity of the Zernike approximation is wavelength dependent as seen in Eq.(2). Based on requiring the coherence patch width to be 1/10 the pupil width or smaller, the Zernike approximation can be shown to be applicable when using wavelengths of 1 nm or shorter, assuming all else being equal. Using the Zernike approximation requires caution

and the validity of Zernike approximation has to be verified before application. Also shown is that pupil aberrations pose significant effect on the spatial coherence distributions at the condenser image-plane when Zernike approximation fails.

References

1. Joseph W. Goodman, *Statistical optics*, (Wiley, New York, 1985).

   Critical illumination: Sec.7.2.1, pp306.

   Zernike approximation: Sec.7.2.2, pp311.

   Van Cittert-Zernike theorem: Sec.5.6, pp207-211.

   Generalized Van Cittert-Zernike theorem: Sec.5.6.4, pp218-222.

   Huygens-Fresnel principle: Sec. 5.4.1, pp196-198. Sec7.1.4, pp296-300.

2. D. T. Attwood, *Soft x-rays and extreme ultraviolet radiation : principles and applications*, (Cambridge University Press, 1999).

3. M. Born and E. Wolf, *Principles of optics: electromagnetic theory of propagation, interference and diffraction of light*, (Cambridge University Press, UK, 1997).

   Zernike approximation: Sec10.5.2, pp522-524.

   Van Cittert-Zernike theorem: Sec10.4.2, pp508-512.

   Displacement theorem: Sec.9.1, pp460-464.

4. F. Zernike, "The concept of degree of coherence and its application to optical problems", *Physica* **V**, 785-95 (1938).

5. C. Chang, P. Naulleau, E. Anderson, D. Attwood, "Spatial coherence characterization of undulator radiation", *Opt. Commun.* **182**, 25-34 (2000).

6. Bernard R. A. Nijboer, *The diffraction theory of aberrations*, (Batavia, 1942). Chapter 4.

7. D. Attwood, P. Naulleau, K.A. Goldberg, E. Tejnil, C. Chang, R. Beguiristain, P. Batson, J. Bokor, E.M. Gullikson, M. Koike, H. Medecki, J. Underwood, Tunable coherent radiation in the soft X-ray and extreme ultraviolet spectral regions, *IEEE J. Quantum Electron.* **35**, 709-20 (1999).

8. A.C. Price, L.B. Sorensen, S.D. Kevan, J. Toner, A. Poniewierski, R. Holyst, Coherent soft-X-ray dynamic light scattering from smectic-A films, *Phys. Rev. Lett.* **82**, 755-8 (1999).

9. P. Naulleau, K.A. Goldberg, S.H. Lee, C. Chang, C. Bresloff, P. Batson, D. Attwood, J. Bokor, Characterization of the accuracy of EUV phase-shifting point diffraction interferometry, *Proc. SPIE* **3331**, 114-23 (1998).

10. P. Naulleau, K.A. Goldberg, S.H. Lee, C. Chang, D. Attwood, J. Bokor, Extreme-ultraviolet phase-shifting point-diffraction interferometer: a wave-front metrology tool with subangstrom reference-wave accuracy, *Appl. Opt.* **38**, 7252-63 (1999).

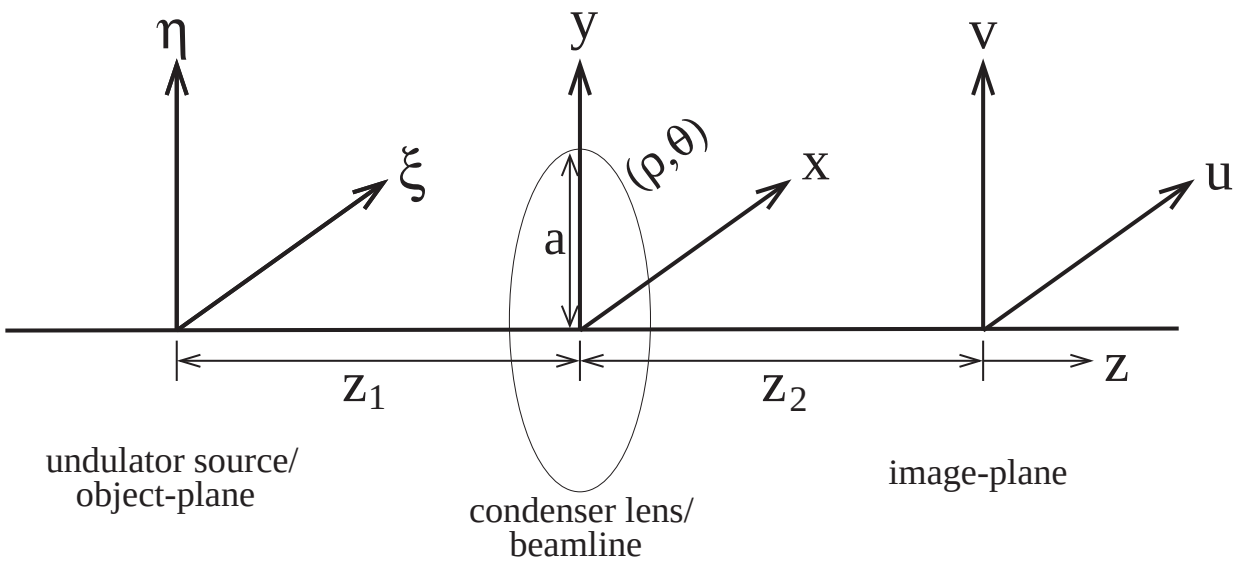

Fig. 1. Coordinate system

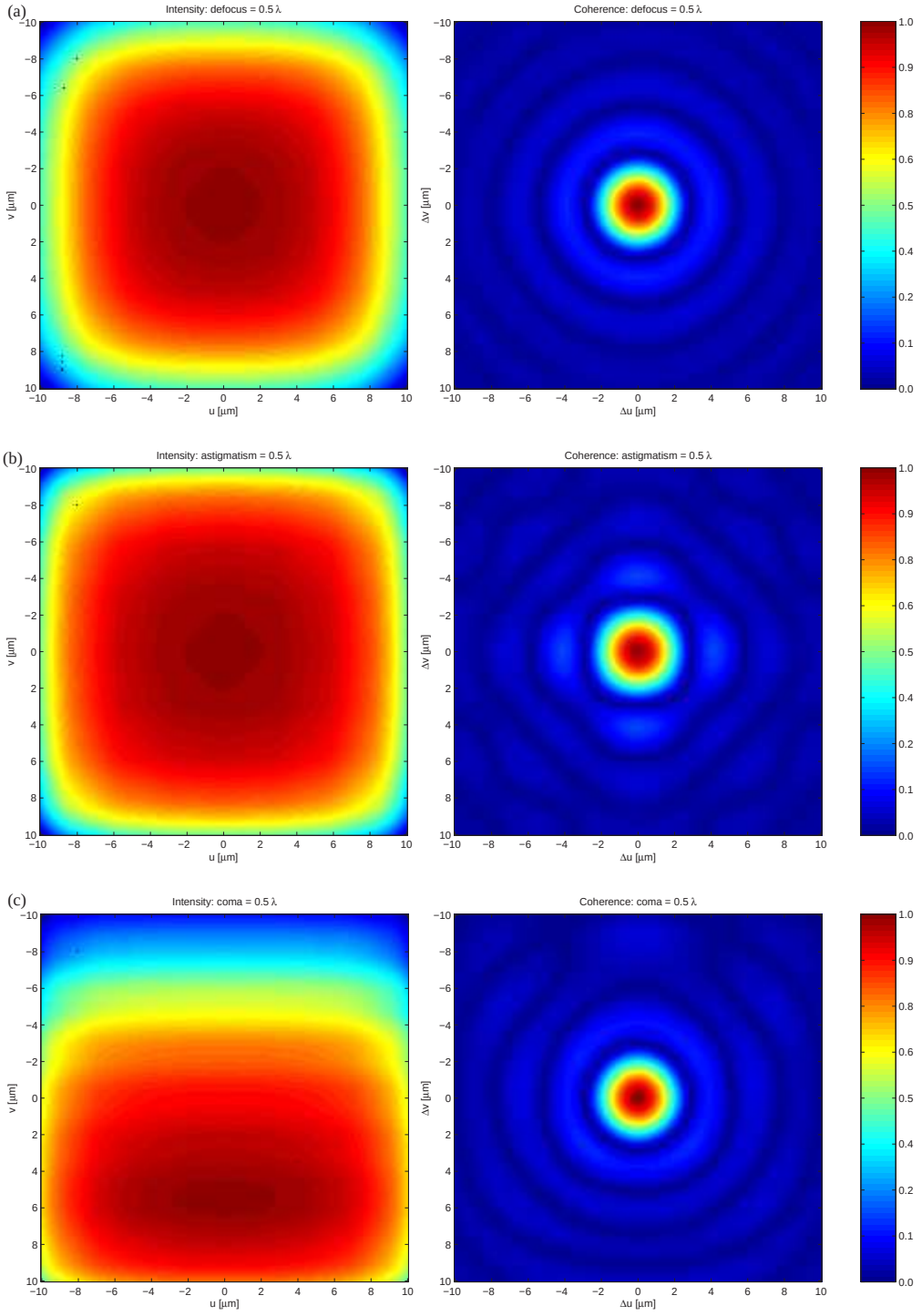

Fig. 2. Simulation results for a large ($1.6\,mm \times 1.6\,mm$) uniform source. Intensity (left column) and coherence (right column) distributions resulting from the various pupil aberrations (**a** defocus, **b** astigmatism, **c** coma). The coherence distributions are all essentially Airy patterns as predicted by the Zernike approximation.

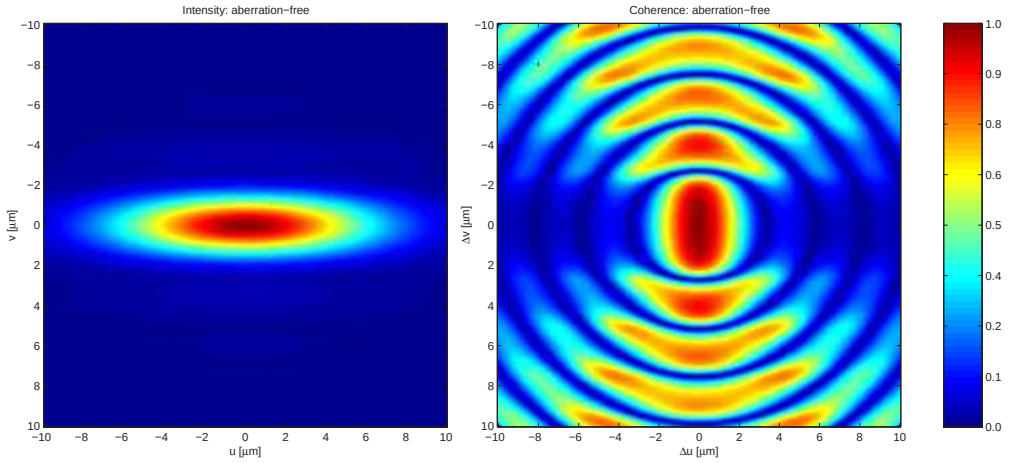

Fig. 3. Simulation results: Intensity and coherence distribution at the condenser image-plane resulting from the un-aberrated condenser pupil and the Gaussian-shaped incoherent source of $(\sigma_x, \sigma_y) = (260\mu m, 16\mu m)$.

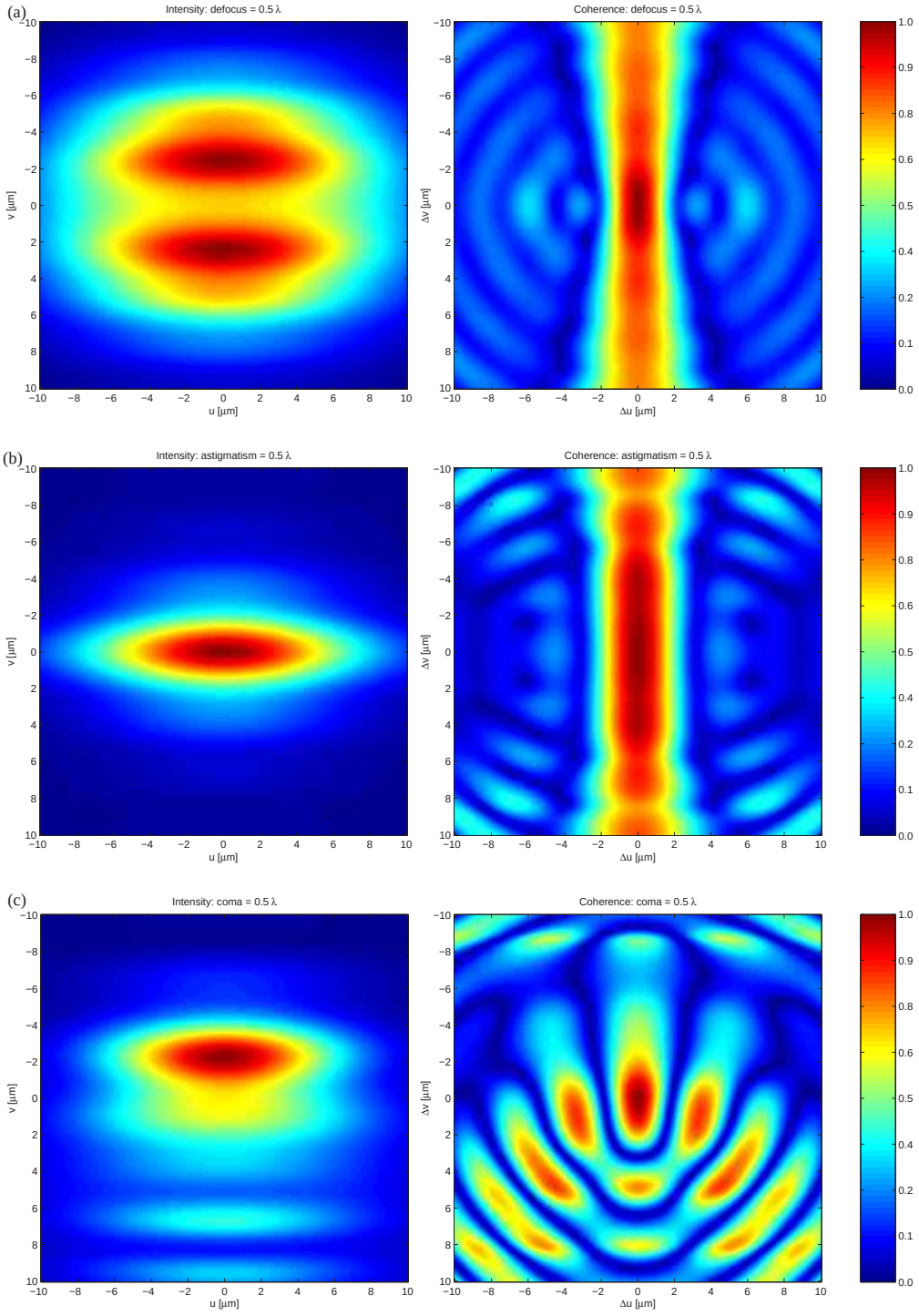

Fig. 4. Simulation results that show the effect of aberrations for the Gaussian-shaped incoherent source: Intensity (left column) and coherence (right column) distribution at resulting from the various aberrations (**a** defocus, **b** astigmatism, **c** coma).